colorants

MDPI

Article

Rock Powder Applied in the Discoloration of Industry Dye of Molded Pulp Packages Effluent

Lariana N. B. Almeida [1,*], Tatiana G. Josué [2], Maria Eduarda K. Fuziki [1], Yuri B. Fávaro [2], Laura S. Ribas [2], Angelo M. Tusset [3], Onélia A. A. Santos [1] and Giane G. Lenzi [2]

[1] Department of Chemical Engineering, State University of Maringá, 5790 Colombo Avenue, Maringá 87080-000, PR, Brazil; mariafuziki@alunos.utfpr.edu.br (M.E.K.F.)
[2] Department of Chemical Engineering, Federal University of Technology Paraná, 330 Doutor Washington Subtil Chueire, Ponta Grossa 84017-220, PR, Brazil; gianeg@utfpr.edu.br (G.G.L.)
[3] Department of Engineering, Federal University of Technology Paraná, 330 Doutor Washington Subtil Chueire, Ponta Grossa 80230-901, PR, Brazil
* Correspondence: beraldolariana@gmail.com

Abstract: In the present work, rock dust was evaluated as an adsorbent and heterogeneous photocatalyst in the discoloration of Basazol Yellow 46 L dye, which is widely used in the dyeing of molded pulp packages. Although rock dust is produced in large quantities in quarries as a byproduct of rock exploration, little is known about its application as a photocatalyst. Rock dust was characterized by XRD, SEM/EDS, photoacoustic spectroscopy, and N_2 physisorption and had its photocatalytic activity assessed through phenol and salicylic acid degradation tests. The characterization results showed that the rock dust is mainly composed of silica and alumina in a triclinic structure, has a bandgap energy of 2.36 eV, and has a specific area of 1.5 m^2/g. Rock dust was proven to be photocatalytically active in phenol and salicylic acid degradation tests and also presented the adsorptive and photocatalytic capacity for the discoloration of effluent containing Basazol Yellow 46 L dye.

Keywords: adsorption; catalyst; dye; silica; packaging

check for updates

Citation: Almeida, L.N.B.; Josué, T.G.; Fuziki, M.E.K.; Fávaro, Y.B.; Ribas, L.S.; Tusset, A.M.; Santos, O.A.A.; Lenzi, G.G. Rock Powder Applied in the Discoloration of Industry Dye of Molded Pulp Packages Effluent. *Colorants* **2023**, *2*, 487–499. https://doi.org/10.3390/colorants2030023

Academic Editor: Anthony Harriman

Received: 8 May 2023
Revised: 28 June 2023
Accepted: 28 June 2023
Published: 7 July 2023

Copyright: © 2023 by the authors. Licensee MDPI, Basel, Switzerland. This article is an open access article distributed under the terms and conditions of the Creative Commons Attribution (CC BY) license (https://creativecommons.org/licenses/by/4.0/).

1. Introduction

Rock dust is the central residue from mineral exploration in quarries involving crushing and cutting rocks [1]. According to statistics published in 2018 by the Brazilian Institute of Geography and Statistics (IBGE), in 2015, there were 996 crushing plants registered in Brazil, most of them in the south and southeast regions. In the same year, the national gravel production was close to 21,749,004 tons, losing only in the mineral production sector to iron ore production [2]. The production of ornamental stones worldwide, according to Montani (2018), is close to 152 megatons per year, with the most prominent world producers being China, India, Turkey, Iran, Brazil, Italy, Egypt, Spain, United States from America, Portugal, France, Saudi Arabia, Greece, and Pakistan [3]. Ornamental stones are rocks that can be used to decorate environments due to their physical and aesthetic characteristics.

Several types of rocks are explored in crushing plants, such as granite, basalt, sandstone, and limestone. During the processing of stones and gravel, rock dust is produced as a byproduct in large quantities and is usually stored in mountains that remain exposed in the quarry's terrain, which can eventually generate dust and cause problems for employees. Although some companies already sell rock dust, the large volume of this byproduct increases the interest in alternative uses.

Research directed at using rock dust as soil fertilizers stands out, as shown in the works of [4,5]. This line of study is not recent and presents many positive results, becoming quite consolidated that rock dust, under the right conditions, serves as a source of nutrients for soils. Another line of research covers the use of rock dust in effluent treatment, as a coagulation aid in water treatment [6]. Adsorption is one of the leading technologies for

pollutants removal [7–11], and in the case of rock dust, the benefits of rock dust for the adsorption of phosphate ions [12] and as a nickel adsorbent [13] can be highlighted.

For the treatment of effluent by heterogeneous photocatalysis (details ahead), few works use rock dust as a catalyst. However, it is possible to highlight that [14] used rock dust combined with MnOx for the degradation, by catalytic ozonation, of oxalic acid. As a result, the authors described that the rock dust material modified with cexadecyl trimethyl ammonium bromide (hydrothermal method) obtained a removal efficiency of approximately 54% of oxalic acid, highlighting that this residue could be used for the treatment of effluent containing the pollutant under study.

Heterogeneous photocatalysis reaction is classified as an advanced oxidative process (AOP), in which a solid semiconductor—rock dust in the present research—suffers electronic excitation under irradiation by absorbing photons with energy greater than or equal to its bandgap energy (Egap). In such conditions, the electrons present in the valence band (VB) are promoted to the conduction band (CB), and a hole (h+) with positive potential is formed in the VB. Water molecules adsorbed on the surface of the photocatalyst can also react with the photogenerated electron/hole pairs, forming hydroxyl radicals (HO•), which subsequently react with the organic pollutant, oxidizing it to CO_2 and H_2O. This reaction is called indirect photocatalysis, whereas in direct photocatalysis, the compounds can be oxidized directly by VB holes [15–17].

Several factors influence the photocatalysis reaction, including pollutant concentration, photocatalyst concentration, temperature, and radiation. It is worth noting that artificial UV radiation minimizes the occurrence of electron–hole pair recombination and generally results in greater efficiency in the degradation of dyes [18].

In the present work, the target pollutant was the cationic dye Basazol Yellow 46 L, widely used to color molded pulp packaging, whose raw material consists of paper, water, and additives. However, as rock dust is a material where little is known about its performance as a photocatalyst, it is not advisable to prove its photocatalytic activity using dyes as a model pollutant. In this sense, [19], when expressing that dyes should not be used to demonstrate the catalytic activity of materials, justified that some dyes, when photoexcited, are capable of donating electrons to the conduction band of a semiconductor, indicating that the radiation emitted by an external source is absorbed by the dye and not by the semiconductor oxide. This behavior can confuse people and lead to wrong and hasty conclusions about the photoactivity of new materials, as is the case of rock dust. As an alternative, the authors mention that carrying out tests separately with phenol and salicylic acid is an excellent option for proving the catalytic activity of a given material, as they provide a general perspective on the role of hydroxyl radicals and the transfer processes of electrons (electron–hole pair) that are commonly described in photocatalysis reactions. Therefore, this research also used phenol and salicylic acid as pollutants.

In this context, the present work aimed to evaluate the degradation of phenol, salicylic acid, and the dye Basazol Yellow 46 L by reactions of heterogeneous photocatalysis, using rock dust as a semiconductor.

2. Materials and Methods

2.1. Materials

The rock dust used throughout the research was collected in a quarry in Castro in Paraná—Brazil. It comes from granite-type rock, and after collection, the material was sieved to obtain a granulometry of less than 0.3 mm and stored at room temperature in plastic containers.

The dye Basazol Yellow 46 L was donated by a company that uses it during the production process of its molded pulp packaging. The dye, in liquid state, has a yellow color, pH of approximately 2, and boiling point of 46 °C.

The dye in this study, C. I Basic Yellow 96, or Basazol Yellow 46 L, is classified as a cyanine-type methine dye [20]. Its complete structure is not available, being the property of the only company that manufactures it, BASF-Solenis. However, the general structure of

Basazol Yellow 46 L is described in [21]. The general structure is shown in Figure 1. Phenol and salicylic acid were supplied by Synth and BIOTEC, respectively.

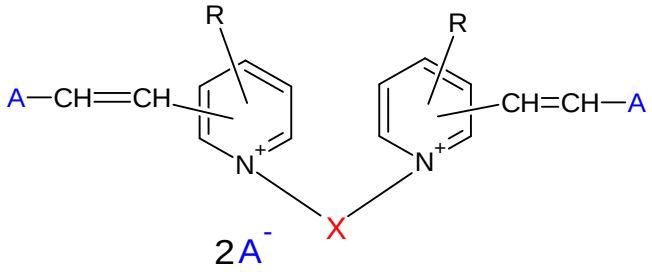


Figure 1. Structure of the methine dye.

2.2. Characterization of Rock Dust

2.2.1. Scanning Electron Microscopy (SEM) Associated with Energy Dispersive Spectroscopy (EDS)

The sample was previously metalized with gold for 10 min, then surface topographic images were obtained using a scanning electron microscope, model VEGA 3 LMU TESCAN (TESCAN, Saint Petersburg, Russia). It has a 30 kV W filament, 3.0 nm resolution, SE, and BSE retractable detectors. The microscope also has an EDS detector, model AZTec Energy X-Act, resolution 130 eV (Oxford, TESCAN, Saint Petersburg, Russia).

2.2.2. X-ray Diffraction (XRD)

For this analysis, a Bruker D8 Advance X-ray diffractometer with MiniFlex 300/600 Goniometer (Bruker, Billerica, MA, USA), from 3° to 90°, with scan speed equal to 2°/min, 40 kV, and 15 mA, was used. The result obtained was then analyzed using standards published by the ICDD (International Center for Diffraction Data), and to calculate the size of the crystallites, Equation (1) was used, initially described by Scherrer in 1918 [22]:

$$L = \frac{K\lambda}{\beta \cos \theta} \quad (1)$$

The size of the crystallite L is calculated from the equation that involves a dimensionless constant (K) whose value depends on the shape of the particle, the wavelength (λ) of the electromagnetic radiation used (Cu K-alpha 1.5406 Å), as a function of full width at half maximum (β), and the Bragg diffraction angle (θ (rad)) [23,24].

2.2.3. Textural Analysis: N_2 Adsorption and Desorption Measurements

In the present work, the nitrogen (N_2) physisorption method at 77 K was used for this characterization, and the equipment used was the Quantachrome Autosorb Automated Gas Sorption System. The specific area was calculated using the BET method [25], and the pore volume and average pore diameter were determined at a relative pressure of 0.99 by the BJH method [26].

2.2.4. Photoacoustic Spectroscopy

The analysis makes it possible to determine the bandgap energy of the materials, that is, the minimum energy necessary for the excitation of electrons. For this, an experimental configuration made in the laboratory was used as described in Drabeski et al. (2020) [27], in which a light source with an 800 W Xenon arc lamp (Oriel, model 66926, Thorlabs, Ottawa, ON, Canada) emitted light for a monochromator (Oriel, model 74100 Cornerstone TM 260 (1/4 m), Thorlabs, Ottawa, ON, Canada). The light modulation frequency was controlled by a mechanical chopper (Stanford Research Systems, model SR 540, Thorlabs, Ottawa, ON, Canada). The microphone coupled to the photoacoustic cell detected the photoacoustic signal. The signal was then transferred to an amplifier (lock-in) that provided the intensity and phase of the photoacoustic signal to a personal computer. The spectra were

normalized with respect to the carbon signal. All photoacoustic spectra were obtained at a modulation frequency of 23 Hz and, to calculate the bandgap energy, Equation (2) was used, described below:

$$\alpha E = A(E - E_g)^m \quad (2)$$

where α is the absorption coefficient, A is a constant independent of the photon energy (E), which is equal to E = hv, where h is Planck's constant (4.13×10^{-15} eV.s), v is the frequency of radiation, E_g is the optical bandgap energy, and the m depends on the type of transition between the bands. Constructing a graph of $(\alpha E)^2$ as a function of photon energy (E), we have the direct bandgap energy from a linear fit at the intersection of the x-axis, that is, when $(\alpha)^2 = 0$ [23,27].

2.2.5. Fourier Transform Infrared Spectroscopy (FTIR)

The rock dust was evaluated before and after the heterogeneous photocatalysis reaction for the discoloration of the effluent containing dye. For the recovery of the material after the reaction, vacuum filtration was performed, and the material retained on the filter paper was subjected to drying in room temperature for 12 h and then drying again at 80 °C for 24 h in an oven with renewal and air circulation SOLAB-SL 102.

The FTIR analysis was performed in infrared spectrophotometer equipment in the middle region with Fourier transform (FT-MIR) performed in the wavenumber range from 4000 to 400 cm^{-1} with a resolution of 4 cm^{-1}, number of accumulations equal to 32 and KBr wafer by transmittance mode.

2.3. Experimental Tests

- For the experimental tests, we used a volume of 500 mL of solution in a reactor with a volume of 600 mL (Figure 2). The reactor was surrounded by a rubber jacket for cooling, with an inlet and outlet for cold water passage. A 250 W mercury vapor lamp was attached just above the reactor, which was open to the environment. Furthermore, the solution was kept under constant magnetic stirring, and airflow was bubbled into the reaction medium at a volumetric flow rate of 0.5 L min^{-1}. Oxygen is widely used in photodegradation processes due to its low cost and because it does not compete for adsorption with the semiconductor present in the medium. The addition of oxygen, for example, can help the reaction by avoiding the recombination of free radicals and aiding in the production of hydroxyl radicals [28,29]. For Teixeira and Jardim, using O_2 in the reaction can decrease the recombination effect of the electron–hole pair since oxygen acts as an electron acceptor.



(**a**) (**b**) (**c**)

Figure 2. Experimental apparatus: (**a**) photocatalysis; (**b**) adsorption; (**c**) photolysis.

The total time for each reaction was 60 min of adsorption (lamp and airflow off) followed by 120 min of photocatalysis (UV irradiation and airflow on).

2.3.1. Discoloration of Effluent Containing Cationic Dye

The synthetic solutions were prepared with distilled water and the liquid dye Basazol Yellow 46 L to obtain a concentration of 10 μL L^{-1}. For the adsorption tests, the reactions proceeded without the cooling jacket, the air bubbling, and the radiation provided by the lamp. For the photolysis reaction, only the presence of rock dust was excluded.

The tests were carried out with industrial effluent collected on three different days in the molded pulp packaging industry in Palmeira in Paraná—Brazil. At the end of the process, it mainly contains dye, paper, water, and additives. For the tests with industrial effluent, the rock dust concentration was set at 6.0 g L^{-1} and the pH at 7, and the tests were carried out in the same way as seen for the synthetic effluent prepared with the same dye.

The residual concentration of the dye was analyzed in a UV–Vis spectrophotometer (Femto-800 XI, Femto, São Paulo, Brazil) in a scan from 200 to 600 nm, with particular attention to the wavelength of 431 nm, characteristic of the target dye, and previously determined using the calibration curve.

2.3.2. Phenol and Salicylic Acid Degradation

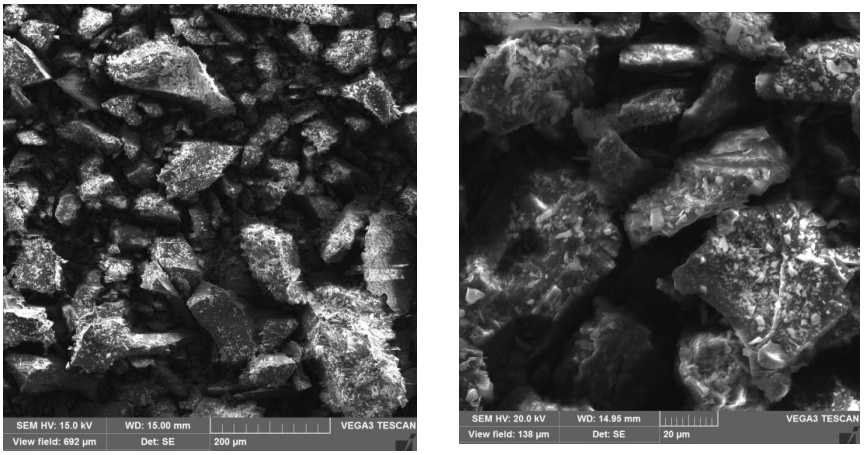
Additional tests were also carried out with phenol and salicylic acid (SA) to verify the photocatalytic activity of the materials used here [19]. The conditions were 50 μmol L^{-1} as initial pollutant concentration (phenol and AS), 1.0 g L^{-1} of catalyst, and pH 7. The samples were collected at determined times, centrifuged, and then the residual concentration of both phenol and salicylic acid were evaluated with high-performance liquid chromatography (HPLC) using a C18 column, eluent 30% acetonitrile and 70% phosphate buffer (pH = 2.8), a flow rate of 1.0 mL min^{-1}, a retention time of 5 min, and wavelength of 210 nm.

3. Results and Discussion

3.1. Rock Dust Characterization

3.1.1. SEM/EDS

From the SEM results (Figure 3), it was possible to observe that the rock dust has an irregular surface whose shape is close to small rocks, and does not have a spherical tendency as do other commonly known photocatalysts, ZnO and TiO_2.



(**a**) (**b**)

Figure 3. SEM images of rock dust: (**a**) 200×; (**b**) 1000×.

The composition of the estimated elemental surface was obtained employing the EDS analysis (energy-dispersive X-ray spectroscopy) presented in Figure 4. It was possible to verify that the elements oxygen (O), silicon (Si), and aluminum (Al) are the main constituents of the surface of the material, collectively representing approximately 90% of the composition. These elements are present in the form of oxides, which are considered

the most stable forms for these elements. More specifically, silicon dioxide (SiO_2), known as silica, and aluminum oxide, called alumina (Al_2O_3), are the predominant forms observed.

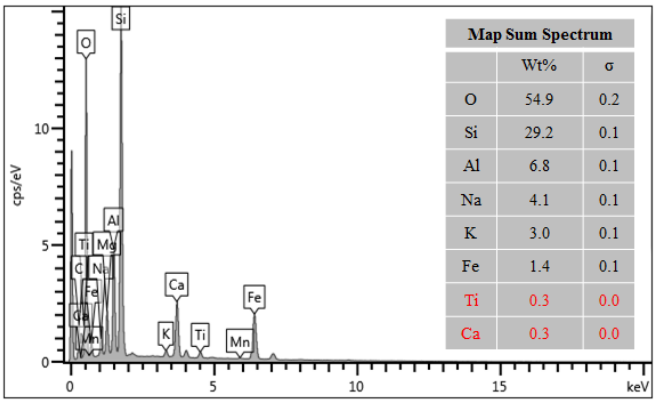


Figure 4. EDS spectrum of rock dust.

The other elements present, together, correspond to 10% of the identified components of rock dust, being sodium (Na), potassium (K), iron (Fe), titanium (Ti), and calcium (Ca).

Both silica and alumina occur naturally and are widely prevalent in minerals such as stones and granites. The rock powder used here (PdR) is a byproduct of granitic rock exploration, and the composition of this type of rock can vary considerably, but, on average, it is made up of approximately 72.4% SiO_2, 14.42% Al_2O_3, 4.12% K_2O, and 3.69% Na_2O [30].

3.1.2. X-ray Diffraction (XRD)

Figure 5 shows the XRD results. The crystalline structure of this material was identified as triclinic. The material showed peaks at values of 2θ around 21,26, 33, 36, 39, 40, 42, 50, 59, 64, 68, 75, 79, and 81° referring to silica (SiO_2), peaks at 13, 22, 24, 25, 17, 30, 32, 45, and 51° refer to albite, and peaks at 13, 21, 22, 23, 24, 27, 41, 55, and 67° refer to microcline. Albite and microcline or microcline are classified as aluminosilicate minerals whose chemical formulas are described as $Na(AlSi_3O_8)$ and $K(AlSiO_4)$, respectively [31]. Potassium aluminosilicates (potassium feldspar, for example, microcline), sodium (sodium feldspar, for example, albite), and calcium (calcium feldspar) comprise a group of minerals called feldspars, and feldspars, together with quartz and mica, constitute the granitic rocks [32], which are the rocks that originated the rock dust.

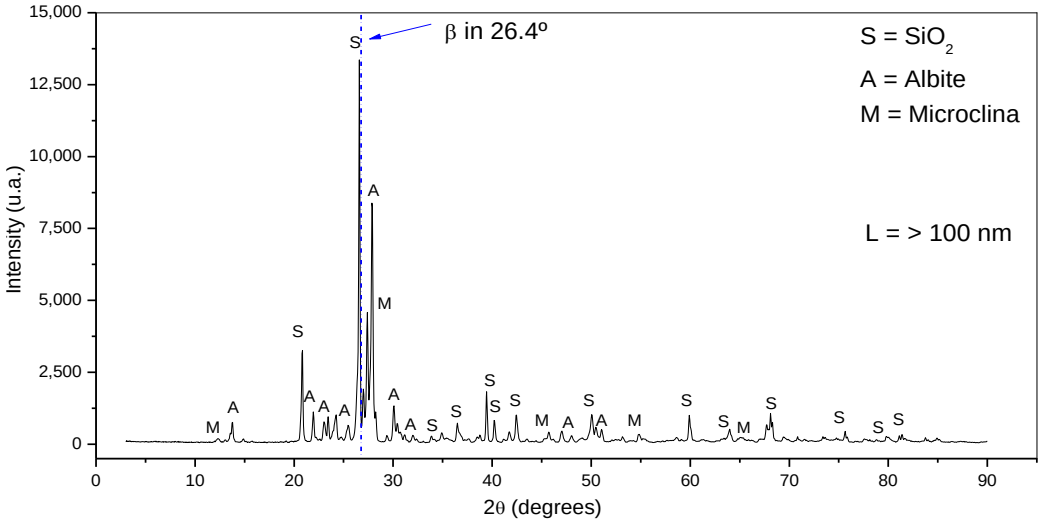


Figure 5. Rock dust diffractograms.

Through the Rietveld refinement of the sample (Figure 6), it was possible to estimate the mass composition of the sample to be approximately 24.9% of SiO_2, 45.3% of albite, and 29.8% of monocline. Table 1 describes the cell parameters estimated from the Rietveld refinement (χ^2 = 3.371).

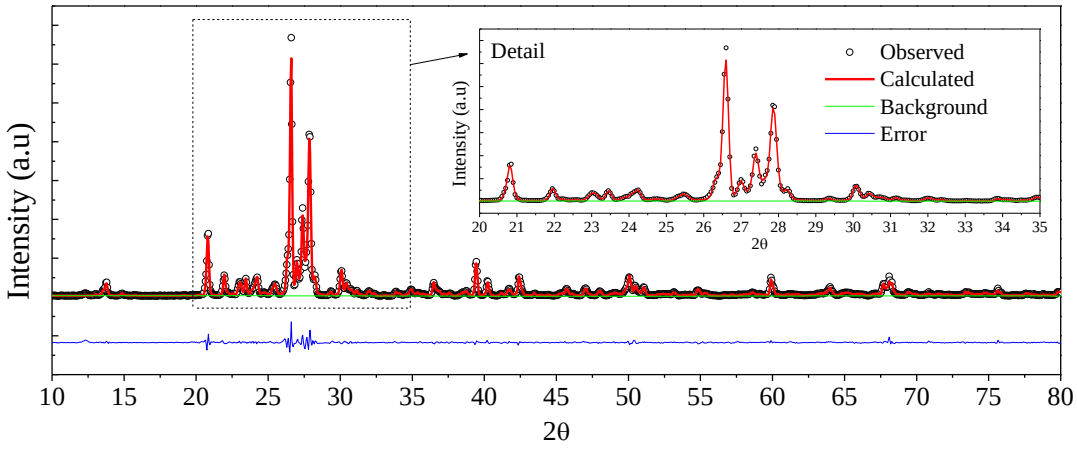


Figure 6. Rietveld refinement of the X-ray diffraction pattern of rock dust sample.

Table 1. Rietveld refinement results and cell parameters. (χ^2 = 3.371).

Phase	a	b	c	α	β	γ	Volume	Mass Fraction
SiO2	4.912	4.920	5.408	90.09	89.951	120.008	113.17	0.24867
Albite	8.141	12.784	7.159	94.263	116.61	87.659	664.244	0.45285
Microcline	8.589	12.983	7.218	90.556	115.904	87.824	723.413	0.29849

3.1.3. Specific Surface Area and Bandgap (E_{gap})

Rock dust can be classified as a mesoporous material according to the behavior of its adsorption isotherm, which can be seen in Figure 7a. Mesoporous materials have a pore diameter between 2 and 50 nm. Furthermore, the specific area of the rock dust approaches 1.5 m^2/g, and this low value is related to the silica in the quartz structure present in large amounts in the material. In the work of [33], an analysis of the specific area of pure quartz sand was also carried out, and the defined value was <1.0 m^2/g, which corresponds to a value close to the one found here (1.5 m^2/g). In the study of [34], the value found for quartz sand was 0.019 m^2/g, much lower than the value found here for rock dust.

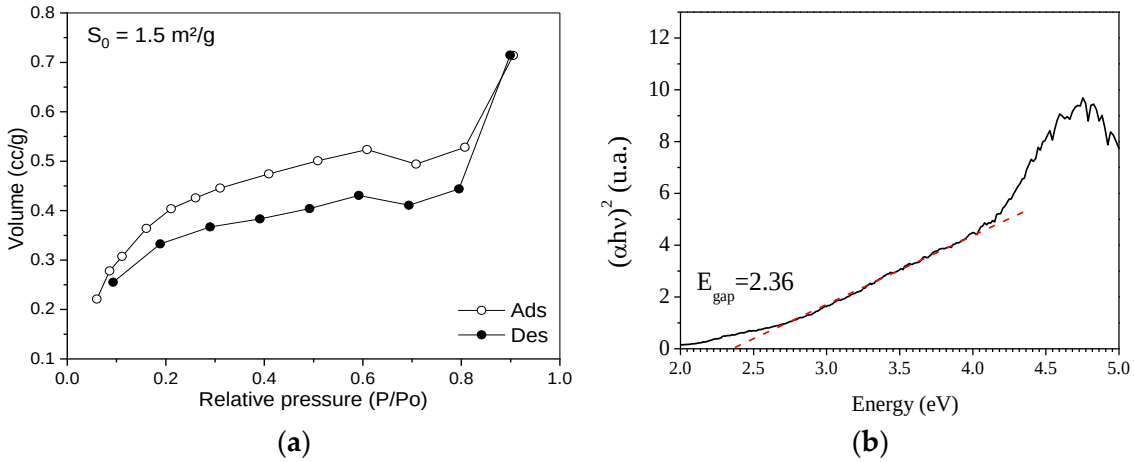


Figure 7. Characterization results: (**a**) N_2 physisorption isotherm and (**b**) photoacoustic spectroscopy.

The result of the photoacoustic spectroscopy, shown in Figure 7b, allowed the estimation of the bandgap (2.36 eV) by the intersection of the linear fit of the energy versus $(\alpha h\nu)^2$ plot with the x-axis. The bandgap energy value of silica nanoparticles defined in the research conducted by [35] was 2.22 eV, being close to the E_{gap} value of the rock dust in the present study, which has, in its composition, mainly silica.

3.1.4. FTIR

The FTIR results are presented in Figure 8 and will be discussed next as the results of the experimental tests are presented.

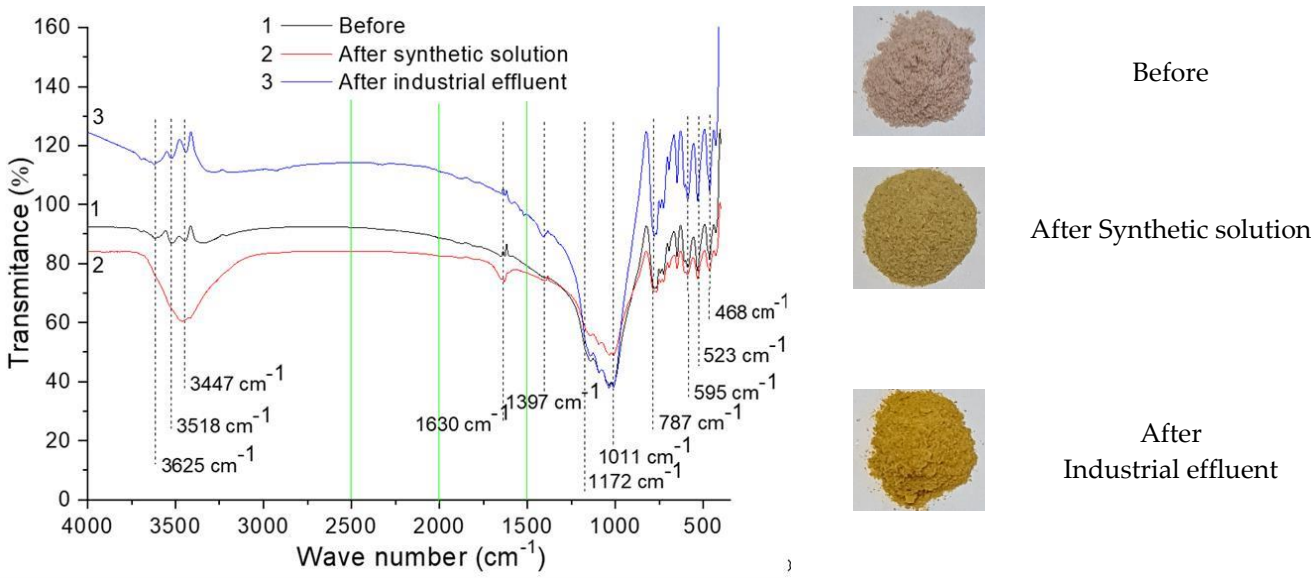


Figure 8. FTIR characterization of rock dust.

3.2. Synthetic and Industrial Dye Degradation

The results of the dye adsorption and photocatalytic discoloration processes in synthetic and industrial effluents are shown in Figures 9 and 10, respectively. It can be observed that for the synthetic effluent, there is negligible adsorption on the catalytic surface (~18%).

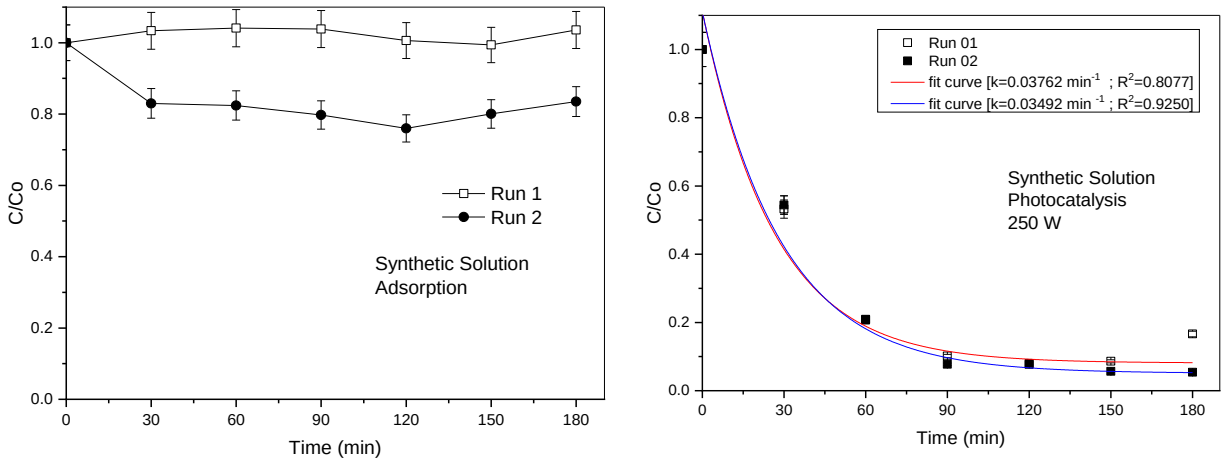
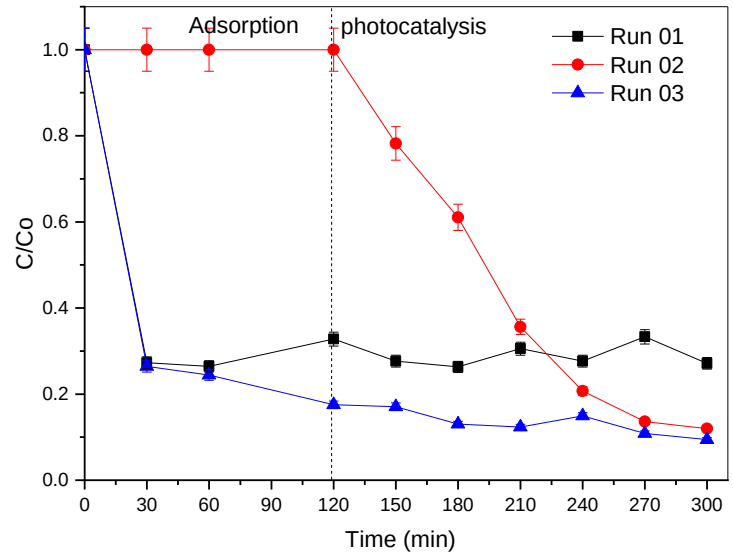
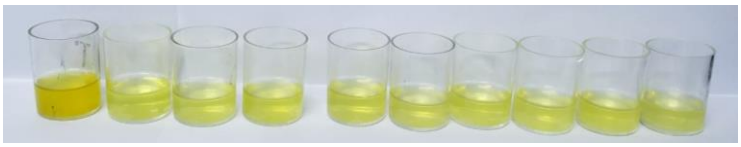


Figure 9. (**a**) Adsorption; (**b**) photocatalysis (1 g L^{-1} of rock dust; pH 7).



(**a**)



(**b**)



(**c**)



(**d**)

Figure 10. Results of (**a**) adsorption and photocatalysis; visual analysis of the process. (**b**) Run 1, (**c**) Run 2, and (**d**) Run 3; industrial effluent (6 g L^{-1} of rock dust; pH 7).

On the other hand, when we start the photocatalytic reaction, the discoloration has a high discoloration speed (Figure 8b). We observed that at around 180 min, the effluent is practically discolored.

The photocatalytic tests with the effluent sample were carried out with rock dust 6 g L^{-1}. This amount of catalyst was determined after photocatalyst tests due to its greater activity/efficiency in dye discoloration. As previously mentioned, industrial effluent contains other compounds, such as dye, paper, water, and additives. The results can be seen in Figure 9.

As shown in Figure 10, the rock dust has a greater adsorption capacity for the dye Basazole Yellow 46 L when present in the industrial effluent. The material offers excellent performance as an adsorbent for two effluent samples and a photocatalytic capacity for one of the samples. The difference in color change can be seen in Figure 10b–d.

This discrepancy in the adsorption capacity of dye present in the real effluent is probably associated with the residual presence of chemical additives introduced in productions before that in which the sample was collected. Thus, it shows a significant

variation in the color and composition of the real effluent, which implies difficulties in its treatment process.

In addition to effluent treatment being a significant challenge for research due to large fluctuations in its composition, as this research used a material that has not yet been explored for this purpose, it becomes difficult to compare with other studies already carried out since the characteristics of each rock vary according to the region and stone explored. Some research using quartz sand, which is the material that comes closest to the features of rock dust, has also identified it as an excellent adsorbent, similar to in Mohammad-Rezaei and Jaymand's research about the adsorption of heavy metals using graphene coated with quartz sand [36]. Tokarsky et al. (2013) [33] evaluated the discoloration of the dye acid orange 7, synthesizing TiO_2 catalysts supported on quartz sand, while Jada et al. (2016) studied methylene blue dye adsorption using quartz sand, obtaining relevant results [37]. The latter used quartz sand naturally, which is very close to the rock dust characteristics in the present study. The results obtained by Jada et al. were promising, leading the authors to conclude that quartz sand can be applied for the adsorption of methylene blue dye when at basic pH and a temperature of 60 °C.

3.3. Degradation of Phenol and Salicylic Acid

In the degradation of salicylic acid using rock dust, Figure 11a shows that in the first 15 min of the reaction, there was slight adsorption of the pollutant in the rock dust. However, soon after possible desorption of the same contaminant, the concentration returns practically to the same value as the initial concentration.

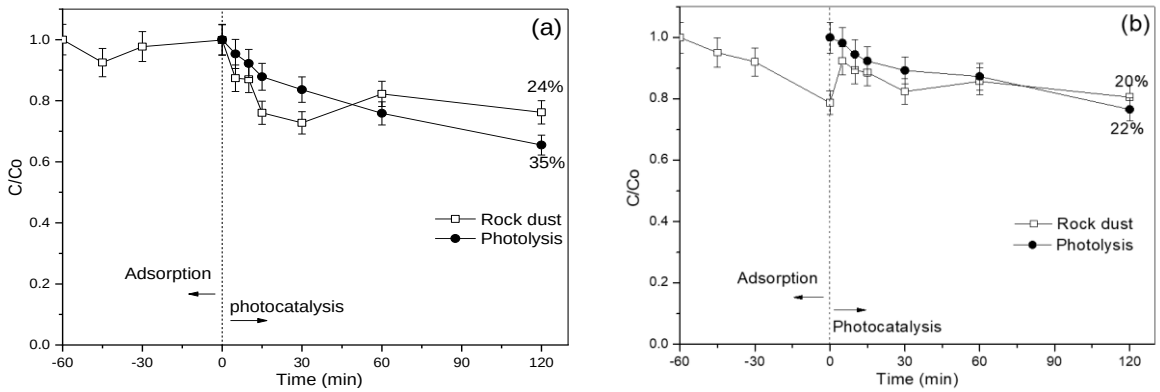


Figure 11. Photoactivity tests of rock dust in the degradation of (**a**) salicylic acid and (**b**) phenol; (catalyst concentration = 1.0 g L^{-1}; pH 7).

In the salicylic acid degradation process using rock dust, Figure 11a shows that at over 60 min of adsorption, there was a pollutant adsorption rate of only 7%. On the other hand, the adsorption of phenol by rock dust reached 20% at the end of 60 min.

In the photocatalytic process, the concentration of salicylic acid presented a fast reaction speed and concentration decrease in the first 30 min. A study by Fuziki et al. (2023) addressed the photocatalytic degradation of acetylsalicylic acid, resulting in salicylic acid and acetic acid formation. After 120 min, the degradation was 24% [38]. In addition, other products were identified throughout the process, such as fumaric acid/maleic acid, malic acid, and malonic acid.

In the case of phenol, represented in Figure 11b, it was observed that, when starting the photocatalysis, there was a reduction in the concentration of the pollutant, but in a similar way to the photolysis reaction conducted in parallel. However, in both cases (salicylic acid and phenol), the kinetics of the photolysis reaction was slower compared to photocatalysis using rock powder.

Comparing the two graphs in Figure 11, the degradation rate using rock dust was higher for salicylic acid (Figure 11a).

Rock dust is still a poorly studied material as a photocatalyst; however, the authors of [39] studied phenol degradation using TiO_2 supported on quartz sand synthesized by the sol–gel method and obtained 90% phenol removal at the end of 350 min, and 30% degradation by photolysis. Furthermore, the researchers also found that by changing some operational variables, such as the initial phenol concentration, there was a change in degradation: an increase in the initial phenol concentration decreased degradation, with the reverse also observed.

The contribution of this work is detailed in the flowchart of Figure 12.

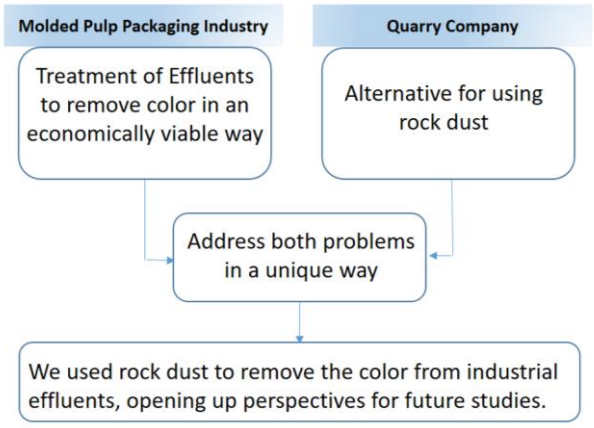


Figure 12. Flowchart with the description of the contribution of this work.

4. Conclusions

Given the results obtained, we verified that the dye Basazol Yellow 46 L could be removed by adsorption and post-heterogeneous photocatalysis using rock dust as a photocatalyst and an adsorbent, respectively. Higher percentages of discoloration were obtained through the photocatalytic reaction for the synthetic solution's discoloration. In contrast, for industrial effluent, both adsorption and photocatalysis promoted the discoloration of the effluent. Therefore, for the discoloration of the industrial effluent, initial treatment with adsorption is suggested, and once the dye has not been removed, the treatment with heterogeneous photocatalysis is continued. This initial adsorption step is necessary since it was observed that only with adsorption can high percentages of discoloration of the effluent be obtained, which does not justify proceeding with the photocatalytic reaction. However, due to the heterogeneity of the effluent, which is related to the composition (variation of dye concentration), as seen in Figure 8b–d, it may happen that only the adsorption is not efficient, which justifies proceeding with the photocatalysis. This article makes a significant contribution by exploring the potential of rock dust as an adsorbent material and photocatalyst. Thus far, few studies have developed in this direction, making this research an original approach. Rock dust, being a low-cost material widely available in Brazil, proves to be promising for the treatment of effluents containing pollutants such as phenol, salicylic acid, and Basazol Yellow 46 L dye of rock in the treatment of other pollutants, as well as to investigate possible improvements in its performance through chemical treatments.

Author Contributions: L.N.B.A., T.G.J., Y.B.F. and L.S.R. carried out the experiment, and conceived and planned the experiments. G.G.L. and A.M.T. performed characterization analysis. G.G.L., M.E.K.F. and O.A.A.S. performed original draft preparation. All authors discussed the results and contributed to the final manuscript. All authors have read and agreed to the published version of the manuscript.

Funding: This research received no external funding.

Institutional Review Board Statement: Not applicable.

Informed Consent Statement: Not applicable.

Data Availability Statement: The data used to support the findings of this study are included within the article. Should further data or information be required, these are available from the corresponding author upon request.

Acknowledgments: The authors thank the Capes, Fundação Araucaria, and CNPq agencies, and analyses were performed at the laboratories LabMult C^{2}MMa—UTFPR—Ponta Grossa and LabMult CA—UTFPR—Pato Branco.

Conflicts of Interest: The authors declare no conflict of interest.

References

1. De Brito, R.S.; Batista, J.F.; Moraes, O.N.K.; da Silva, S.O. Rochagem Na Agricultura: Importância e Vantagens Para Adubação Suplementar. *South Am. J. Basic Educ. Tech. Technol.* **2019**, *6*, 528–540.
2. Deparamento Nacional de Produção Mineral. *Cadastro Nacional de Produtores de Brita*; Pinheiro, C.G.W.F., Ed.; Deparamento Nacional de Produção Mineral: Brasília, Brazil, 2018.
3. Montani, C. Marble and Stones in the World 2018 XXIX Report. *Miner. Econ.* **2019**, *32*, 255–256.
4. Ramos, C.G.; Hower, J.C.; Blanco, E.; Oliveira, M.L.S.; Theodoro, S.H. Possibilities of Using Silicate Rock Powder: An Overview. *Geosci. Front.* **2021**, *13*, 101185. [CrossRef]
5. Lopes, O.M.M.; Carrilho, E.N.V.M.; Lopes-Assad, M.L.R.C. Effect of Rock Powder and Vinasse on Two Types of Soils. *Rev. Bras. Ciências Solo* **2014**, *38*, 1547–1557. [CrossRef]
6. De Oliveira Zawadzki, R.A.F.; Vieira, A.R.; Zanella, F.S.; dos Santos, P.B. Uso Do Pó de Rocha Para Tratamento Físico-Químico de Efluentes-Auxipó. In Proceedings of the II Congresso Brasileiro de Rochagem, Poços de Caldas, Brazil, 12–17 May 2013; pp. 359–367.
7. Li, X.-G.; Ma, X.-L.; Sun, J.; Huang, M.-R. Powerful Reactive Sorption of Silver(I) and Mercury(II) onto Poly(o -Phenylenediamine) Microparticles. *Langmuir* **2009**, *25*, 1675–1684. [CrossRef] [PubMed]
8. Meesri, S.; Praphairaksit, N.; Imyim, A. Extraction and Preconcentration of Toxic Metal Ions from Aqueous Solution Using Benzothiazole-Based Chelating Resins. *Microchem. J.* **2007**, *87*, 47–55. [CrossRef]
9. Abollino, O.; Giacomino, A.; Malandrino, M.; Mentasti, E. The Efficiency of Vermiculite as Natural Sorbent for Heavy Metals. *Appl. Contam. Soil. Water Air Soil. Pollut.* **2007**, *181*, 149–160. [CrossRef]
10. Li, X.-G.; Huang, M.-R.; Jiang, Y.-B.; Yu, J.; He, Z. Synthesis of Poly(1,5-Diaminonaphthalene) Microparticles with Abundant Amino and Imino Groups as Strong Adsorbers for Heavy Metal Ions. *Microchim. Acta* **2019**, *186*, 208. [CrossRef]
11. Li, X.G.; Huang, M.R.; Tao, T.; Ren, Z.; Zeng, J.; Yu, J.; Umeyama, T.; Ohara, T.; Imahori, H. Highly Cost-Efficient Sorption and Desorption of Mercury Ions onto Regenerable Poly(m-Phenylenediamine) Microspheres with Many Active Groups. *Chem. Eng. J.* **2020**, *391*, 123515. [CrossRef]
12. Ahmed, N.A.S.; Latif, M.L.A.; Sanad, S.A.; Sanad, S.A.; Mohammed, S.A.R. Utilization of Industrial Granitic Waste as Adsorbent for Phosphate Ions from Wastewater. *Int. J. Sci. Eng. Res.* **2020**, *11*, 184–194.
13. Park, J.H.; Lee, J.K. Weathered Sand of Basalt as a Potential Nickel Adsorbent. *Processes* **2020**, *8*, 1238. [CrossRef]
14. Zhang, L.; Wei, L.; Ling, L.; Chen, Z.; Jia, Y.; Zhang, H.; Li, Z.; Guo, J. Preparation of Wasted Rock Dust Catalyst and Its Catalytic Ozonation Properties for the Treatment of Oxalic Acid Containing Wastewater. *Mater. Sci. Forum* **2019**, *956*, 273–281. [CrossRef]
15. Braslavsky, S.E.; Braun, A.M.; Cassano, A.E.; Emeline, A.V.; Litter, M.I.; Palmisano, L.; Parmon, V.N.; Serpone, N. Glossary of Terms Used in Photocatalysis and Radiation Catalysis (IUPAC Recommendations 2011). *Pure Appl. Chem.* **2011**, *83*, 931–1014. [CrossRef]
16. Herrmann, J. Photocatalysis Fundamentals Revisited to Avoid Several Misconceptions. *Appl. Catal. B* **2010**, *99*, 461–468. [CrossRef]
17. Ziolli, R.L.; Jardim, W.F. Mechanism Reactions of Photodegradation of Organic Compounds Catalyzed by TiO_2. *Quim. Nova* **1998**, *21*, 319–325.
18. Reza, K.M.; Kurny, A.; Gulshan, F. Parameters Affecting the Photocatalytic Degradation of Dyes Using TiO_2: A Review. *Appl. Water Sci.* **2017**, *7*, 1569–1578. [CrossRef]
19. Barbero, N.; Vione, D. Why Dyes Should Not Be Used to Test the Photocatalytic Activity of Semiconductor Oxides. *Environ. Sci. Technol.* **2016**, *50*, 2130–2131. [CrossRef]
20. Knutson, K.; Kirzan, S.; Ragauskas, A. Enzymatic Biobleaching of Two Recalcitrant Paper Dyes with Horseradish and Soybean Peroxidase. *Biotechnol. Lett.* **2005**, *27*, 753–758. [CrossRef]
21. Degen, H.-J.; Feichtmayr, F.; Grychtol, K. Methine Dyes for Paper and Amonically-Modified Fibers. US4256458A, 17 March 1981.
22. Scherrer, P. Bestimmung Der Grösse Und Der Inneren Struktur von Kolloidteilchen Mittels Röntgenstrahlen, Nachrichten von Der Gesellschaft Der Wissenschaften, Göttingen. *Math.-Phys. Kl.* **1918**, *2*, 98–100.
23. Fuziki, M.E.K.; Abreu, E.; De Carvalho, A.E.; Silva, L.H.B.O.; Fidelis, M.Z.; Tusset, A.M.; Brackmann, R.; Dias, D.T.; Lenzi, G.G. Sol–Gel Fe/TiO_2 Magnetic Catalysts Applied to Selenium Photoreduction. *Top Catal.* **2020**, *63*, 1131–1144. [CrossRef]
24. Lim, D.J.; Marks, N.A.; Rowles, M.R. Universal Scherrer Equation for Graphene Fragments. *Carbon* **2020**, *162*, 475–480. [CrossRef]
25. Brunauer, S.; Emmett, P.H.; Teller, E. Adsorption of Gases in Multimolecular Layers. *J. Am. Chem. Soc.* **1938**, *60*, 309–319. [CrossRef]

26. Barrett, E.P.; Joyner, L.G.; Halenda, P.P. The Determination of Pore Volume and Area Distributions in Porous Substances. *I. Comput. Nitrogen Isotherms. J. Am. Chem. Soc.* **1951**, *73*, 373–380. [CrossRef]
27. Drabeski, R.G.; Gunha, J.V.; Novatski, A.; de Souza, G.B.; Tebcherani, S.M.; Kubaski, E.T.; Dias, D.T. Raman and Photoacoustic Spectroscopies of SnO2 Thin Films Deposited by Spin Coating Technique. *Vib. Spectrosc.* **2020**, *109*, 103094. [CrossRef]
28. De Almeida Barêa Teixeira, C.P.; de Figueiredo Jardim, W. *Processos Oxidativos Avançados: Conceito Teóricos*; Caderno Temático; Universidade Estadual de Campinas—UNICAMP: Campinas, Brazil, 2004; Volume 3.
29. Yasmina, M.; Mourad, K.; Mohammed, S.H.; Khaoula, C. Treatment Heterogeneous Photocatalysis; Factors Influencing the Photocatalytic Degradation by TiO_2. *Energy Procedia* **2014**, *50*, 559–566. [CrossRef]
30. Sharma, S.B.; Kumar, B. Effects of Stone Crusher Dust Pollution on Growth Performance and Yield Status of Rice (*Oryza sativa* L.). *Int. J. Curr. Microbiol. Appl. Sci.* **2016**, *5*, 796–806. [CrossRef]
31. Mookherjee, M.; Mainprice, D.; Maheshwari, K.; Heinonen, O.; Patel, D.; Hariharan, A. Pressure Induced Elastic Softening in Framework Aluminosilicate- Albite (NaAlSi3 O8). *Sci. Rep.* **2016**, *6*, 34815. [CrossRef]
32. Da Luz, A.B.; Coelho, J.M. Rochas e Minerais Industriais—19. Feldspato. In *Rochas & Minerais Industriais: Usos e Especificações*; CETEM: Rio de Janeiro, Brazil, 2005.
33. Tokarský, J.; Matějka, V.; Neuwirthová, L.; Vontorová, J.; Mamulová Kutláková, K.; Kukutschová, J.; Čapková, P. A Low-Cost Photoactive Composite Quartz Sand/TiO_2. *Chem. Eng. J.* **2013**, *222*, 488–497. [CrossRef]
34. Hanaor, D.A.H.; Sorrell, C.C. Sand Supported Mixed-Phase TiO_2 Photocatalysts for Water Decontamination Applications. *Adv. Eng. Mater.* **2014**, *16*, 248–254. [CrossRef]
35. Arunmetha, S.; Vinoth, M.; Srither, S.R.; Karthik, A.; Sridharpanday, M.; Suriyaprabha, R.; Manivasakan, P.; Rajendran, V. Study on Production of Silicon Nanoparticles from Quartz Sand for Hybrid Solar Cell Applications. *J. Electron. Mater.* **2018**, *47*, 493–502. [CrossRef]
36. Mohammad-Rezaei, R.; Jaymand, M. Graphene Quantum Dots Coated on Quartz Sand as Efficient and Low-Cost Adsorbent for Removal of Hg^{2+} and Pb^{2+} from Aqueous Solutions. *Environ. Prog. Sustain. Energy* **2019**, *38*, S24–S31. [CrossRef]
37. Jada, A.; Ait Akbour, R.; Douch, J. Surface Charge and Adsorption from Water onto Quartz Sand of Humic Acid. *Chemosphere* **2006**, *64*, 1287–1295. [CrossRef]
38. Fuziki, M.E.K.; Ribas, L.S.; Tusset, A.M.; Brackmann, R.; Dos Santos, O.A.A.; Lenzi, G.G. Pharmaceutical Compounds Photolysis: PH Influence. *Heliyon* **2023**, *9*, e13678. [CrossRef]
39. Tasbihi, M.; Ngah, C.R.; Aziz, N.; Mansor, A.; Abdullah, A.Z.; Teong, L.K.; Mohamed, A.R. Lifetime and Regeneration Studies of Various Supported TiO_2 Photocatalysts for the Degradation of Phenol under UV-C Light in a Batch Reactor. *Ind. Eng. Chem. Res.* **2007**, *46*, 9006–9014. [CrossRef]

Disclaimer/Publisher's Note: The statements, opinions and data contained in all publications are solely those of the individual author(s) and contributor(s) and not of MDPI and/or the editor(s). MDPI and/or the editor(s) disclaim responsibility for any injury to people or property resulting from any ideas, methods, instructions or products referred to in the content.